Viscosity and mutual diffusion of deuterium-tritium mixtures in the warm-dense-matter regime

J. D. Kress,[1] James S. Cohen,[1] D. A. Horner,[1] F. Lambert,[2] and L. A. Collins[1]
[1]*Theoretical Division, Los Alamos National Laboratory, Los Alamos, New Mexico 87545, USA*
[2]*CEA, DAM, DIF, F-91297 Arpajon, France*
(Received 7 June 2010; published 14 September 2010)

We have calculated viscosity and mutual diffusion of deuterium-tritium (DT) in the warm, dense matter regime for densities from 5 to 20 g/cm^3 and temperatures from 2 to 10 eV, using both finite-temperature Kohn-Sham density-functional theory molecular dynamics (QMD) and orbital-free molecular dynamics (OFMD). The OFMD simulations are in generally good agreement with the benchmark QMD results, and we conclude that the simpler OFMD method can be used with confidence in this regime. For low temperatures (3 eV and below), one-component plasma (OCP) model simulations for diffusion agree with the QMD and OFMD calculations, but deviate by 30% at 10 eV. In comparison with the QMD and OFMD results, the OCP viscosities are not as good as for diffusion, especially for 5 g/cm^3 where the temperature dependence is significantly different. The QMD and OFMD reduced diffusion and viscosity coefficients are found to depend largely, though not completely, only on the Coulomb coupling parameter Γ, with a minimum in the reduced viscosity at $\Gamma \approx 25$, approximately the same position found in the OCP simulations. The QMD and OFMD equations of state (pressure) are also compared with the hydrogen two-component plasma model.

DOI: 10.1103/PhysRevE.82.036404 PACS number(s): 52.25.Fi, 52.65.Yy, 52.27.Cm, 52.27.Gr

I. INTRODUCTION

The deuterium-tritium (DT) reaction is the most accessible for terrestrial fusion reactors. Magnetic confinement operates at relatively high temperatures and low densities, but inertial confinement proceeds through the warm dense matter (WDM) regime, which encompasses temperatures from a few thousand Kelvin (~1 eV) to a few million Kelvin (~100 eV) and densities from a few hundredths solid (~10^{21} atoms/cm^3) to hundreds of times solid (~10^{25} atoms/cm^3). In the compression of the inertial-confinement-fusion capsules, heavy elements are used to drive enclosed shells and the light fuel. In the course of the compression, impurities such as plastics, beryllium, or copper, as well as heavy metals such as gold are inadvertently or deliberately (as diagnostics) mixed into the fuel and can have a considerable impact on the burn efficiency. The outcomes may be strongly altered by the nature of the mixing and plasma instabilities. The viscosity and mutual diffusion in the mixture are important input properties for hydrodynamic modeling treating the stability of initial interfaces and the degree of fuel contamination [1–3]. Modeling such environments requires an integrated approach in order to follow the many interaction paths and constituents that arise in these complicated concoctions. The development of methods that treat electrons quantum mechanically coupled with molecular dynamics for the nuclear motion of large samples of atoms has enabled for considerable progress in the detailed understanding of these regimes. Since these types of calculations are computationally demanding, it is important to thoroughly explore and benchmark the methods on simple mixtures before launching into generating large amounts of data for complicated mixtures as described above. One of the simplest in this regard involves mixtures of hydrogen isotopes.

To this end, transport properties of deuterium-tritium (*D-T*) mixtures are determined in the present work by quantum molecular-dynamics (QMD) simulations, which treat the electrons quantum mechanically through finite-temperature density-functional theory (FTDFT), as well as in orbital-free molecular-dynamics (OFMD) simulations, which treat the kinetic energy of the electrons semiclassically and thereby are able to reach higher temperatures. Both treat the nuclear motions classically. Previous QMD simulations include the determination of self-diffusion coefficients in the pure H system [4–7] and mutual diffusion for isotopic mixtures [6,8] for temperatures $T=1$ to 5 eV and equivalent H mass densities of $\rho=0.1$ to 1.0 g/cm^3.[1] Both self-diffusion and viscosity were determined using QMD for the isotope *D* for temperatures up to 4.3 eV and equivalent H mass densities 0.17 to 0.37 g/cm^3 [9]. Previous OFMD simulations include the pioneering work of Zérah *et al.* [10] in determining self-diffusion coefficients for pure H. More recently, OFMD simulations of self-diffusion have been performed on much heavier elements (Fe, Au) [11,12] and on mixtures of Li and H [13]. The present work extends the previous QMD studies on transport properties to higher temperatures (up to $T=10$ eV) and to higher densities (equivalent H mass density between 2 and 8 g/cm^3) and provides a comprehensive comparison with OFMD simulations as well as with kinetic theory and one- and two-component plasma (OCP and TCP) theories and simulations.

The paper is organized as follows. First the formalism for quantum and orbital-free MD and for determining the static and transport properties are described. Then, viscosities, diffusion coefficients, and equations of state (pressures) for deuterium-tritium mixtures are presented, and the QMD and OFMD results are compared with the results from simpler, reduced models. Finally, a few concluding remarks are given.

[1]Note: 1 mol/cm^3 particle density=1 g/cm^3 hydrogen mass equivalent.

II. FORMALISM

A. Quantum molecular dynamics

Our QMD simulations for *D-T* employed the Vienna *ab-initio* Simulation Package (VASP) [14–16], in which the electrons are treated fully quantum mechanically using a plane-wave FTDFT description. The electron-ion interaction is represented by a projector augmented wave (PAW) pseudopotential. The ions are evolved classically according to the forces from the electron density and the ion-ion repulsion. The system is assumed to be in local thermodynamic equilibrium with the electron and ion temperatures equal ($T_e=T_i=T$). In our simulations, the electron temperature is fixed, and the ion temperature is kept at this value through simple velocity rescaling (Woodcock thermostat) or Nosé-Hoover thermostat [17].

At each time step t for a periodically replicated cell of volume V containing N_e active electrons and N_i ions in fixed spatial positions $\mathbf{R}(t)$, we first perform a FTDFT calculation within the Kohn-Sham (KS) construction [18] to determine a set of electronic state functions $[\Psi_{i,\mathbf{k}}(\mathbf{r},t)|i=1,N_b]$ and eigenenergies $\epsilon_{i,\mathbf{k}}$ at each k-point $\mathbf{k}$,

$$H_{\mathrm{KS}}\Psi_{i,\mathbf{k}}(\mathbf{r},t)=\epsilon_{i,\mathbf{k}}\Psi_{i,\mathbf{k}}(\mathbf{r},t) \tag{1}$$

where in atomic units

$$H_{\mathrm{KS}}=-\frac{1}{2}\nabla^2+V_{\mathrm{ext}}(\mathbf{r})+\int\frac{n_e(\mathbf{r}')}{|\mathbf{r}-\mathbf{r}'|}d\mathbf{r}'+V_{\mathrm{xc}}(\mathbf{r}) \tag{2}$$

with

$$n_e(\mathbf{r})=2\sum_i|\Psi_{i,\mathbf{k}}(\mathbf{r},t)|^2. \tag{3}$$

These terms represent the kinetic energy, the external or electron-ion interaction, the Hartree contribution to the electronic energy, and the exchange-correlation potential, respectively.

The ions are then advanced with a velocity Verlet algorithm, based on the forces due to the other ions and electronic density, to obtain a new set of positions and velocities. Repetition of these two steps propagates the system in time yielding a trajectory consisting of the positions and velocities $[\mathbf{R}(t),\mathbf{V}(t)]$ of the ions and a collection of state functions $[\Psi_{i,\mathbf{k}}(\mathbf{r},t)]$ for the electrons.

All our simulations employed only Γ point ($\mathbf{k}=0$) sampling of the Brillouin zone and 216 atoms—108 atoms each of *D* and *T* (of mass 2 and 3 amu, respectively) in a cubic cell of length *L* (volume $V=L^3$). We solve the KS equations within the generalized gradient approximation [19] and describe the hydrogen-electron interaction with a PAW with a maximum energy cutoff of 700 eV. An examination of the pair correlation functions and nearest-neighbor lists for typical simulations indicate that few encounters occur within the PAW core even for the densest case. A sufficient number N_b of bands was included such that the occupation of the highest band was less than 10^{-3}. Trajectories were evolved with a time step of 0.1 fs.

B. Orbital free molecular dynamics

We also investigated the *D-T* mixture under the same physical conditions using OFMD simulations [11,20–22]. In this scheme, the kinetic energy of the electrons is treated in a semiclassical approximation, up to first order in the partition function of the electrons. The orbital-free electronic free energy at ion positions $\mathbf{R}$ is given by

$$F_e[\mathbf{R},n_e]=\frac{1}{\beta}\int d\mathbf{r}\left(n_e(\mathbf{r})\Phi[n_e(\mathbf{r})]-\frac{2\sqrt{2}}{3\pi^2\beta^{3/2}}I_{3/2}(\Phi[n_e(\mathbf{r})])\right)+\int d\mathbf{r}V_{\mathrm{ext}}(\mathbf{r})n_e(\mathbf{r})+\frac{1}{2}\int\int d\mathbf{r}d\mathbf{r}'\frac{n_e(\mathbf{r})n_e(\mathbf{r}')}{|\mathbf{r}-\mathbf{r}'|}+F_{\mathrm{xc}}[n_e] \tag{4}$$

where $\beta=1/k_BT$ and I_ν is the Fermi integral [23] of order ν. The screened potential $\Phi[n_e(\mathbf{r})]$ is related to the electronic density $n_e(\mathbf{r})$ by [22]

$$n_e(\mathbf{r})=\frac{\sqrt{2}}{\pi^2\beta^{3/2}}I_{1/2}(\Phi[n_e(\mathbf{r})]); \tag{5}$$

charge conservation requires that $\int d\mathbf{r}n_e(\mathbf{r})$ equals the total electronic charge.

The first integral in Eq. (4), which depends only on the local electronic density n_e in the true spirit of the Hohenberg-Kohn theorem [24], is the well-known finite-temperature Thomas-Fermi expression [25]. The exchange-correlation term $F_{\mathrm{xc}}[n_e]$ is expressed in the local density approximation of Perdew and Zunger [26,27]. For this study, we omit the von Weiszäcker correction and work in a Thomas-Fermi-Dirac form using the formula proposed by Perrot [28] to deal with the kinetic-entropic part. The divergence of the electron-nucleus potential is regularized at each thermodynamic condition through a procedure that closely follows the production of the norm-conserving pseudopotential for QMD [12]. The cutoff radius is chosen to be 30% of the Wigner-Seitz radius in order to prevent the overlap of regularization spheres. The number of plane waves describing the local electronic density is then adjusted to converge the thermodynamic properties to within less than 1%.

The chain of calculation of the OFMD procedure is similar to that of QMD. At each time step, the electronic free energy is minimized in terms the local electronic density and the nuclei are propagated according to their electrostatic interactions arising from both nuclei and electrons. The molecular dynamics is performed in the isokinetic ensemble [29], and the time step is computed from the thermal velocity of the nuclei and the Wigner-Seitz radius [30]. The orbital-free procedure treats all electrons on an equal footing, albeit approximately, with no distinction between bound and ionized electrons.

C. Static and transport properties

The total pressure of the system, given by

$$P=n_ik_BT+P_e, \tag{6}$$

where n_i is the ion number density and k_B is the Boltzmann constant, is the sum of the ideal gas pressure of the ions and

the electronic pressure P_e computed via the electronic forces. The electronic pressure is averaged over the trajectory after the system has equilibrated.

The self-diffusion coefficient D_α for species α can be computed from the trajectory by the mean-square displacement

$$D_\alpha^{(R)} = \frac{1}{6t}\langle|\mathbf{R}_{\alpha i}(t) - \mathbf{R}_{\alpha i}(0)|^2\rangle \tag{7}$$

or by the velocity autocorrelation function

$$D_\alpha^{(V)} = \frac{1}{3}\int_0^\infty \langle \mathbf{V}_{\alpha i}(t)\cdot\mathbf{V}_{\alpha i}(0)\rangle \mathrm{d}t, \tag{8}$$

where $\mathbf{R}_{\alpha i}$ ($\mathbf{V}_{\alpha i}$) is the position (velocity) of the ith particle of species α. This quantity is computed for both D and T.

These two formulations of the self-diffusion coefficients are formally equivalent only in the long-time limit. We have generated trajectories of sufficient temporal length to reach times such that the velocity autocorrelation function becomes zero and contributes no further to the integral, and the mean-square displacement away from the origin consistently fits to a straight line. The values obtained from these two approaches generally lie within one percent of each other, so we report only one value, designated D_α.

We also compute the mutual-diffusion coefficient

$$D_{\alpha\beta} = \lim_{t\to\infty} \overline{D_{\alpha\beta}}(t) \tag{9}$$

from the autocorrelation function (Green-Kubo relation)

$$\overline{D_{\alpha\beta}}(t) = \frac{Q}{3Nx_\alpha x_\beta}\int_0^t \langle A(0)A(t')\rangle \mathrm{d}t' \tag{10}$$

where

$$A(t) = x_\beta \sum_{i=1}^{N_\alpha} \mathbf{v}_i(t) - x_\alpha \sum_{j=1}^{N_\beta} \mathbf{v}_j(t), \tag{11}$$

x_α and N_α denote the concentration and particle number of species α, respectively, and $N=\Sigma_\alpha N_\alpha$. The quantity Q represents the thermodynamic factor related to the second derivative of the Gibbs free energy with respect to concentrations [31], which for an ideal binary fluid is unity. For our simulations, we also set $Q=1$ since studies with Leonard-Jones and other model potentials have shown that even for dissimilar constituents the Q-factor departs from unity by only about 10% [32]. On the other hand, models of plasmas based on point ionic charges in a neutralizing background have indicted that the Q-factor can depart from unity for components with different charges and concentrations [33]. However, for the case treated here of DT ($Z_1=Z_2=1$) at equal concentrations, the estimate of the Q-factor for this plasma model also yields unity. We apply the ideal binary liquid convention only to the determination of Q and include all cross-correlation terms in the evaluation of the integrand of Eq. (10).

The viscosity

$$\eta = \lim_{t\to\infty} \bar{\eta}(t), \tag{12}$$

is computed from the autocorrelation function of the off-diagonal component of the stress tensor [34]

$$\bar{\eta}(t) = \frac{V}{k_B T}\int_0^t \langle P_{12}(0)P_{12}(t')\rangle \mathrm{d}t'. \tag{13}$$

We averaged the results for the five independent off-diagonal components of the stress tensor P_{xy}, P_{yz}, P_{zx}, $(P_{xx}-P_{yy})/2$, and $(P_{yy}-P_{zz})/2$.

Unlike the self-diffusion coefficient, which involves single-particle correlations and attains significant statistical improvement from averaging over the particles, the viscosity and mutual diffusion depend on the entire system and therefore require very long trajectories in order to gain statistical accuracy. We have previously found [13] that empirical fits to the integrals of the autocorrelation functions can substantially shorten the length of the trajectory required. In turn, extrapolation of the fits to $t\to\infty$ can more effectively determine the basic dynamical properties. Both the partial integrals of the velocity autocorrelation function, Eq. (10), and the off-diagonal stress-tensor autocorrelation function $\bar{\eta}(t)$, Eq. (13), have been fit to the functional form $A[1-\exp(t/\tau)]$, where A and τ are free parameters with A giving the resulting property, Eqs. (9) or (12), in the $t\to\infty$ limit. Fitting to this form at short-time integrations produces reasonable approximations to η and $D_{\alpha\beta}$. This fitting procedure also aids in damping the long-time variation.

The fractional statistical error in computing a correlation function C for molecular-dynamics trajectories [35] is given by

$$\frac{\Delta C}{C} = \sqrt{\frac{2\tau}{T_{\mathrm{traj}}}}, \tag{14}$$

where T_{traj} is the length of the trajectory and τ is the correlation, or e-folding, time of the function, calculated from the fit or from interrogations of the function itself. In the previous work [13], we generally fitted over a time interval of $[0,4\tau-5\tau]$. In the present work, we generally fit over the interval $[0,0.8\tau-1.2\tau]$. This shorter interval emphasizes the fit in the region where the function varies most quickly. Furthermore, as t increases the statistics become poorer since there are fewer time origins to sum over when constructing the autocorrelation function [34]. In Fig. 1, the molecular-dynamics results for viscosity at a density of 5 $\mathrm{g/cm^3}$ and temperatures of 3, 5, and 10 eV are displayed with their fits. These particular examples employed a trajectory of length 20 000 and correlation times between 100 and 200 fs. For the viscosity and mutual-diffusion coefficients, the computed error is 10% or less. A total uncertainty of ~20% is estimated by experience due to the fitting procedure and extrapolation to infinite time. Finally, the error in the self-diffusion coefficient remains less than 1% since the particle average gives an additional $1/\sqrt{N}$ advantage.

We have also tested the sensitivity of the QMD simulations to the form of the isokinetic thermostat. The results presented in the figures and tables were determined with ve-

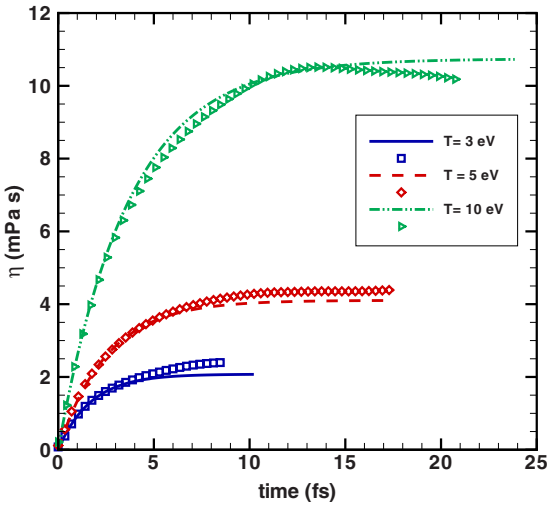

FIG. 1. (Color online) Viscosity as a function of time at a density 5 g/cm^3 and temperatures 3 (squares), 5 (diamonds), and 10 (triangles) eV. The fits (lines) were performed for a sample window of $[0,2\tau]$ and the data points are displayed out to 5τ.

locity rescaling. In addition, we performed several representative simulations with the VASP package using the Nosé-Hoover option. We have compared self-diffusion, mutual-diffusion, and viscosity at 5 eV and 5 g/cm^3 and at 10 eV and 12.5 g/cm^3 and found very small differences between the results from these two thermostats. The viscosities and mutual diffusion differed by 5% or less while the self-diffusion coefficients remained within 1%. In addition, microcanonical tests showed only a 7% departure from the velocity rescaling results for viscosity.

III. RESULTS AND DISCUSSION

We first performed *ab initio* quantum-mechanical simulations with the FTDFT method to benchmark the dynamic properties of the *D-T* mixture in the WDM regime. QMD and OFMD results for the mutual-diffusion coefficient and viscosity, at densities of 5.0 and 12.5 g/cm^3, are shown in Figs. 2 and 3, respectively. (The QMD results are also given in Table I.) The OFMD results are in generally good agreement (10% or better) with the QMD results. The greatest difference of 13% is seen in the viscosity at the highest density and temperature in Fig. 3(b). The error bars displayed are the statistical contribution only, given by Eq. (14). The results are also compared in Figs. 2 and 3 with some simple formulas derived from models. These models all depend only on the dimensionless coupling constant

$$\Gamma = \frac{Z^2 e^2}{a k_B T}, \tag{15}$$

where Z is the ion charge[2] and

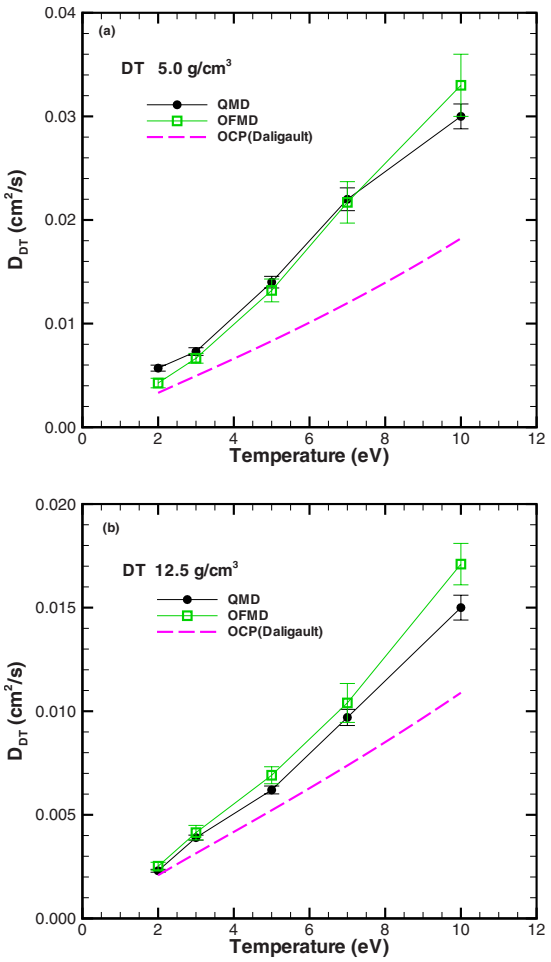

FIG. 2. (Color online) Mutual-diffusion coefficient for the *D-T* mixture as a function of temperature at densities of 5.0 g/cm^3 (top panel) and 12.5 g/cm^3 (bottom panel). Solid circles are QMD calculations; open squares are OFMD calculations; dashed curve is the OCP calculation of Daligault [36]. The error bars on the QMD and OFMD calculations are statistical only [Eq. (14)].

$$a = \left(\frac{3}{4\pi n_i}\right)^{1/3} \tag{16}$$

is the Wigner-Seitz radius of the ions for ion number density n_i. Γ for DT is shown in Fig. 4 for the temperatures and densities considered in Figs. 2 and 3. Dense plasmas are often characterized by the three dimensionless parameters: Γ, the reduced Wigner-Seitz radius

$$r_s = a/a_0 \tag{17}$$

($a_0 \equiv \hbar^2/m_e e^2$ is the Bohr radius), and the degree of Fermi degeneracy

$$\Theta = k_B T/E_F, \tag{18}$$

where

[2]In the binary ionic mixture model [39], the effective charge $Z_{\rm eff}$ is given by $Z_{\rm eff}^2 = \langle Z\rangle_{\rm av}^{1/3}\langle Z^{5/3}\rangle_{\rm av}$ (where $\langle q\rangle_{\rm av} \equiv x_1 q_1 + x_2 q_2$ for any quantity q and number concentrations x_1 and x_2 such that $x_1 + x_2 = 1$), which makes no change in the present case since $Z_1 = Z_2$.

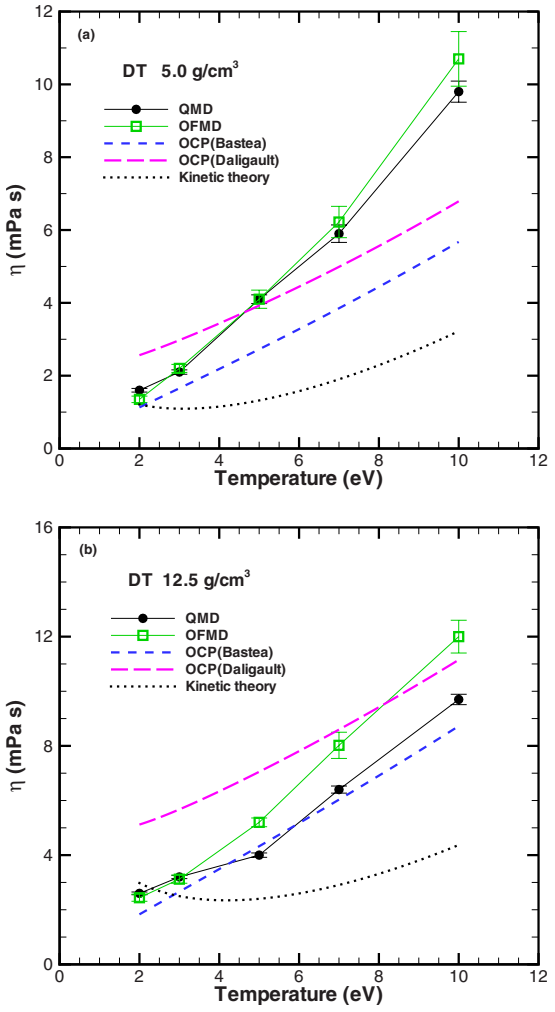

FIG. 3. (Color online) Viscosity of the *D-T* mixture as a function of temperature at densities of (a) 5.0 g/cm^3 and (b) 12.5 g/cm^3. Solid circles are QMD calculations; open squares are OFMD calculations; short-dashed curve is the OCP calculation of Bastea [37]; long-dashed curve is the OCP calculation of Daligault [36]; dotted curve is the fit of Wallenborn and Baus [38] to kinetic theory. The error bars on the QMD and OFMD calculations are statistical only [Eq. (14)].

$$E_F = \hbar^2 \frac{(3\pi^2 n_i Z)^{2/3}}{2m_e} \tag{19}$$

is the (nonrelativistic) Fermi energy of the electrons. Only two of these three parameters are independent.

It is convenient to express the self-diffusion coefficient D as a dimensionless quantity

$$D^* = \frac{D}{\omega_p a^2}, \tag{20}$$

where

$$\omega_p = (4\pi n_i/M)^{1/2} Ze \tag{21}$$

is the plasma frequency for ions of mass M. For the 50:50 *D-T* mixture considered in this work, we use the "hydrodynamic" mixture [37] approximation $M=(2+3)/2=2.5$ amu.

Hansen *et al.* [40] have used a memory-function analysis of the velocity autocorrelation function to obtain the diffusion coefficient for the classical OCP, which they fit to

$$D^* = 2.95\Gamma^{-1.34}. \tag{22}$$

Unfortunately, this fit is not very accurate for $\Gamma \lesssim 4$, corresponding to temperatures greater than 4 eV in Fig. 2. More recently, Daligault [36] has generated a more accurate fit to OCP simulations. As shown in Fig. 2, the agreement of the Daligault fit for DT (using $M=2.5$) with the QMD and OFMD simulations is good at low temperatures (2 and 3 eV). However, as temperature increases, the OCP results disagree more, e.g., underestimating the QMD and OFMD results by $\sim$30% at $T=10$ eV. For densities smaller than those considered in the present work, Clérouin and Dufrêche [9] found that OCP results also lie below the QMD results for the diffusion coefficient by about a factor of 3 for hydrogen mass density equivalents of 0.17 and 0.25 g/cm^3 and temperatures between 10 000 and 50 000 K.

Using a Yukawa potential to add screening to the OCP, Murillo [41] has suggested modifying Γ in Eq. (15) to

$$\Gamma_{\rm mod} = A(\kappa) + B(\kappa)\Gamma + C(\kappa)\Gamma^2, \tag{23}$$

where the coefficients are a parametric function of the inverse screening length κ. When we take $\kappa = 1/\lambda_{\rm TF}$, where

$$\lambda_{\rm TF} = \left(\frac{\pi}{12Z}\right)^{1/3} \sqrt{r_s}, \tag{24}$$

and apply Eq. (23) to the OCP results we find that the screened results based on the Daligault OCP results are up to a factor of 2 times larger than the QMD results for $\rho = 5$ g/cm^3 and 2 to 3 times larger for $\rho = 12.5$ g/cm^3.

Now we turn to the viscosity of the *D-T* mixture. It is convenient to express the viscosity η as a dimensionless quantity

$$\eta^* = \frac{\eta}{n_i M \omega_p a^2}. \tag{25}$$

Bastea [37] has performed classical molecular-dynamics simulations of the OCP and fits his results to the form

$$\eta^* = A\Gamma^{-2} + B\Gamma^{-s} + C\Gamma \tag{26}$$

with $s=0.878$, $A=0.482$, $B=0.629$, and $C=0.001\,88$. Bastea's results, which agree with most other simulations [42–44], are shown in Fig. 3. They are in good agreement with the QMD viscosity at the higher density but up to a factor of 2 too small at the lower density. It is reasonable that the OCP model works better at higher densities since the degeneracy is higher (Θ smaller). The viscosities of Daligault [36], also obtained with classical MD simulations of the OCP, are significantly higher than the other OCP simulations [37,42–44]. The disagreement with the other OCP results is greater than the expected uncertainties in the calculations, and the reason for the difference is uncertain. In both cases the Yukawa screening modification worsens the agreement with the QMD/OFMD results.

Wallenborn and Baus [38] have treated the viscosity of a strongly coupled ($\Gamma > 1$) OCP using kinetic theory. The

TABLE I. QMD results for the *D-T* mixture. The given error bars (Δ) are statistical only [Eq. (14)]. The total uncertainty due to the fitting procedure and extrapolation to infinite time is estimated by experience to be ~20%. Numbers in brackets represent powers of ten.

ρ (g/cm^3)	k_BT (eV)	D (cm^2/s)	ΔD (cm^2/s)	η (mPa s)	$\Delta\eta$ (mPa s)	P_{el} (GPa)
5.0	2	5.7[−3]	2.9[−4]	1.6	0.05	1300
5.0	3	7.3[−3]	3.7[−4]	2.1	0.06	1370
5.0	5	1.4[−2]	5.6[−4]	4.1	0.12	1520
5.0	7	2.2[−2]	1.1[−3]	5.9	0.24	1720
5.0	10	3.0[−2]	1.2[−3]	9.8	0.29	2040
12.5	2	2.3[−3]	6.9[−5]	2.6	0.05	8070
12.5	3	3.9[−3]	1.2[−4]	3.2	0.06	8270
12.5	5	6.2[−3]	1.9[−4]	4.0	0.08	8570
12.5	7	9.7[−3]	3.9[−4]	6.4	0.13	8900
12.5	10	1.5[−2]	6.0[−4]	9.7	0.19	9520

theory uses equilibrium properties as input. Their results are approximated assuming free-particle dynamics by the form

$$\eta^* = \lambda I_1(\lambda) + \frac{[1+\lambda I_2(\lambda)]^2}{\lambda I_3(\lambda)}, \tag{27}$$

where I_1, I_2, and I_3 are parameterized in terms of $\lambda = \frac{4}{3}\pi(3\Gamma)^{3/2}$. The viscosities given by this formula are shown in Fig. 3. For $\rho=5$ g/cm^3, the QMD and OFMD results agree to within statistical uncertainty for all temperatures considered. For $\rho=12.5$ g/cm^3, the OFMD results are ~25% greater than the QMD results for the highest temperature of 10 eV. For $\rho=5$ g/cm^3, Eq. (26) and the kinetic theory agree with QMD at $T=2$ eV while Daligault's result is ~40% larger. However, as the temperature increases, Eq. (26), the results of Daligault, and the kinetic theory all underestimate the QMD results (e.g., by factors of 1.5, 1.7, and 3.2, respectively, at $T=10$ eV). At the higher density of 12.5 g/cm^3, Eq. (26) and the kinetic theory agree with the QMD results at $T=2$ eV, whereas the Daligault OCP results are about a factor of two larger. As the temperature increases, Eq. (26) tracks the QMD results, whereas the Daligault OCP results are somewhat too large. The kinetic theory underestimates the viscosity by a factor of two at 10 eV.

For densities smaller than those considered in the present work, Clérouin and Dufrêche [9] found that QMD viscosities for hydrogen mass density equivalents of 0.17, 0.25, and 0.37 g/cm^3 agree with kinetic theory for temperatures between 1000 and 10 000 K. However, for temperatures between 10 000 and 50 000 K, the kinetic theory underestimates the QMD results (for example, by a factor of about 2 at 50 000 K), as we have observed here for higher densities.

Figure 5(a) shows the electronic pressure P_{el} calculated by QMD and OFMD as a function of temperature for two densities. At density 5 g/cm^3, the QMD electronic pressure is 10–14 % smaller than the OFMD electronic pressure. At density 12.5 g/cm^3 the QMD electronic pressure is 5% smaller than the OFMD electronic pressure. Figure 5(b) shows an estimate of the excess pressure P_{ex}, due to electron exchange and correlation, as a function of density. The excess pressure is not given directly by the QMD or OFMD simulation, but was determined by subtracting the Fermi pressure P_0 of the free-electron gas from the total electronic pressure P_{el} found in these simulations, i.e.,

$$P_{ex} = P_{el} - P_0. \tag{28}$$

The Fermi pressure P_0 of the free-electron gas is given by

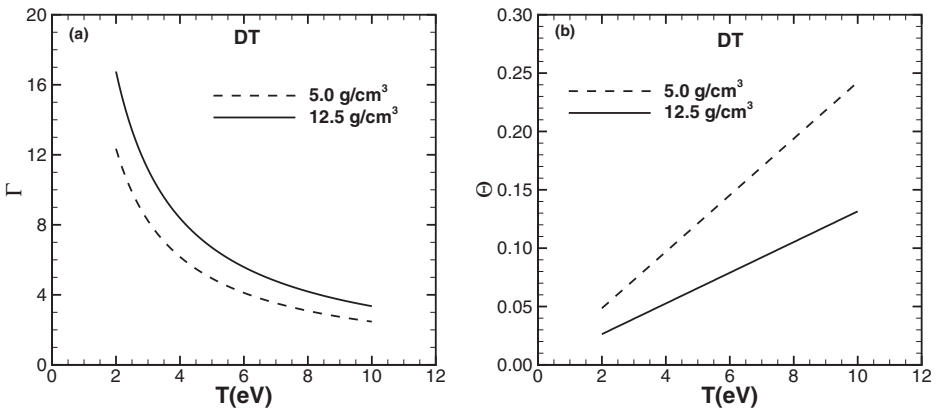

FIG. 4. Dimensionless plasma parameters (a) Γ and (b) Θ for the *D-T* mixture as a function of temperature at densities of 5.0 g/cm^3 (dashed curve) and 12.5 g/cm^3 (solid curve). The third parameter r_s is 1.1018 at 5 g/cm^3 and 0.8118 at 12.5 g/cm^3, independent of T.

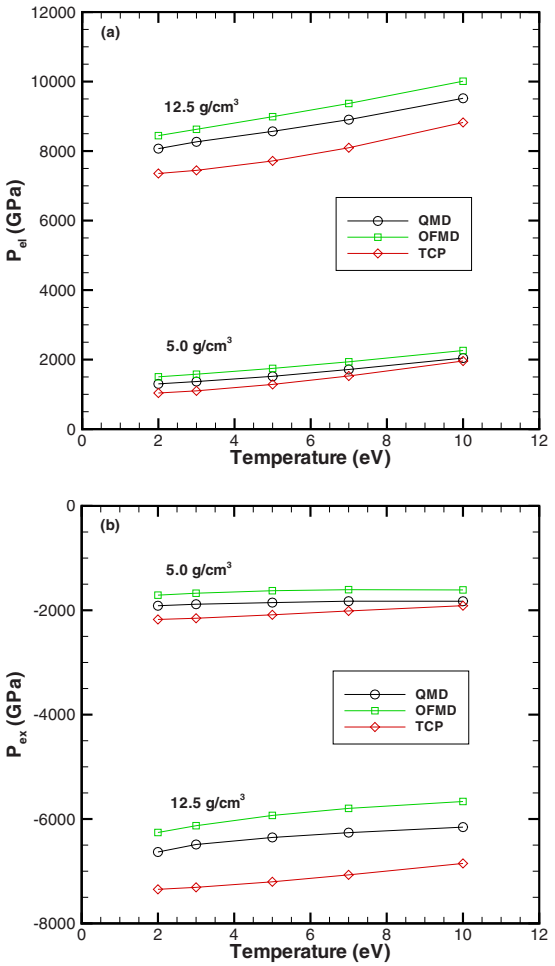

FIG. 5. (Color online) Comparison of the electronic pressures of the *D-T* mixture, obtained from QMD (circles), OFMD (squares), and TCP (diamonds) as a function of temperature at densities of 5.0 g/cm^3 and 12.5 g/cm^3: (a) the total electronic pressure; (b) the excess pressure after the free-electron gas contribution [23] has been subtracted.

$$P_0 = k_B T n_e \Theta^{3/2} I_{3/2}(\alpha), \tag{29}$$

where α is determined by solving the normalization condition

$$I_{1/2}(\alpha) = \frac{2}{3}\Theta^{-3/2}, \tag{30}$$

with Θ given by Eq. (18) [23]. At the values of the degeneracy parameters shown in Fig. 4 this pressure is fairly close to the pressure for a completely degenerate gas. The excess pressure, defined thusly, is generally negative due to exchange and correlation effects. Another estimate of the excess pressure was obtained by differentiating with respect to volume the fit of Ichimaru *et al.* [45] of the excess free energy of the two-component plasma. The corresponding total electronic pressure was obtained by adding P_0 to this value and is shown in Fig. 5(a) for comparison with the QMD and OFMD values. The QMD values lie approximately midway between the OFMD and TCP values.

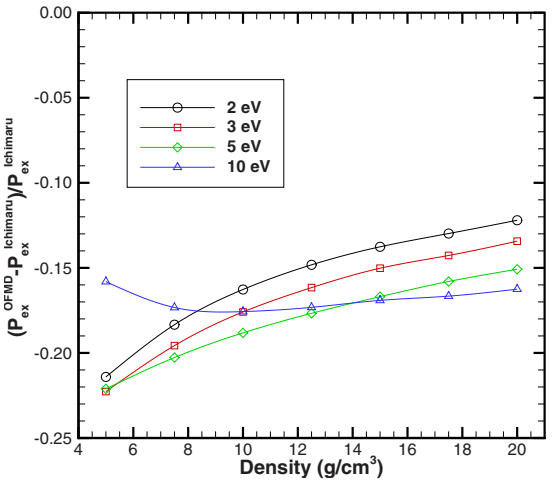

FIG. 6. (Color online) Fractional differences of the OFMD excess pressures from the fit of Ichimaru *et al.* [45] for the hydrogen two-component plasma as a function of density at temperatures of 2, 3, 5, and 10 eV.

Additional simulations for higher densities have been carried out using OFMD. These results are shown in Figs. 6–8. The deviation from the TCP excess pressures, obtained by differentiating the excess free energy fit of Ichimaru *et al.* [45] for the hydrogen two-component plasma, is shown in Fig. 6. The OFMD excess pressures are 12–22 % smaller (in magnitude) than those given by the TCP model. The greatest deviations occur at low densities.

The self-diffusion coefficients shown in Fig. 7(a), calculated from the results of the mixture simulations, have been scaled to remove the trivial mass dependence (scale factor $=\sqrt{M/2.5}$, where $M=2$ for D and $M=3$ for T). For a fixed density, the self-diffusion coefficient rises with temperature as the atoms become more mobile. On the other hand, for a given temperature, the diffusion declines with increasing density, reflecting the greater confinement of the atoms. Even the scaled diffusion of the lighter deuterium is slightly greater than that of the heavier tritium though the two are barely distinguishable at temperatures below about 5 eV. The mutual-diffusion coefficient, calculated from the autocorrelation function of the full *D-T* mixture, is shown in Fig. 7(b). Since self-diffusion coefficients converge much more rapidly than the mutual-diffusion coefficients with respect to the trajectory length, we calculate the average of the self-diffusion coefficients (D_D and D_T) and test whether this is a good approximation to the mutual-diffusion coefficient. In Fig. 7(b) we see that the average [46] is a good approximation at all densities and temperatures considered. Note that the *D-T* mixture is a special case for obtaining the mutual-diffusion coefficient in this manner; the average self diffusion need not be a reasonable approximation to the mutual diffusion in a mixture of atoms with widely different charges and masses.

The viscosity for the *D-T* mixture calculated by the OFMD method is shown in Fig. 8. Viscosity increases with increasing temperature as well as with increasing density in this WDM regime.

Finally we address the question as to what extent the reduced diffusion coefficient D^* and the reduced viscosity η^*

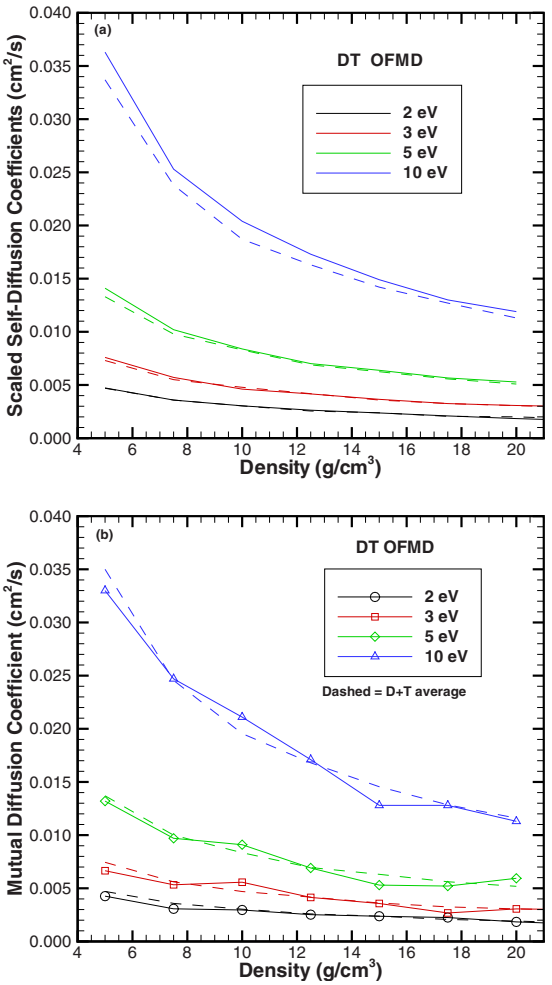

FIG. 7. (Color online) Diffusion coefficients for DT calculated by OFMD as a function of density at temperatures of 2, 3, 5, and 10 eV (lowest to highest curve). Top panel shows the mass-scaled self-diffusion coefficients for pure D (solid curve) and pure T (dashed curve), scaled by a factor $\sqrt{M/2.5}$ where $M=2$ for D and $M=3$ for T. Bottom panel shows the mutual-diffusion coefficient for the D-T mixture; the dashed curve is the average of the D and T results shown in the top panel.

depend only on Γ and not on the density and temperature separately. Plots of the reduced quantities are shown in Figs. 9 and 10. Both agree reasonably well with the OCP model, which depends only on Γ (the OCP viscosities of Daligault [36] are higher than those of the other three calculations [37,43,44]). In the case of the viscosity, the OFMD reduced viscosity has a minimum at $\Gamma \approx 25$, in between the values where the two OCP calculations [36,37] found the minimum but with a smaller magnitude than both. Other models [43,47] have predicted that the minimum occurs at somewhat lower values of Γ.

IV. CONCLUSIONS

We have calculated the diffusion and viscosity of the D-T mixture using the OFMD method for temperatures between 2 and 10 eV and densities between 5 and 20 g/cm^3. The

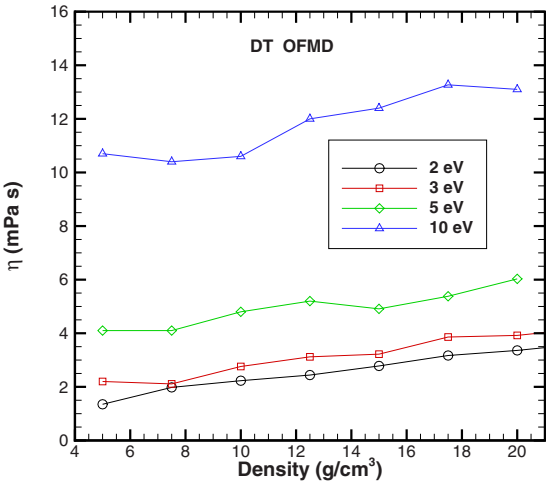

FIG. 8. (Color online) Viscosity for the D-T mixture calculated by OFMD as a function of density at temperatures of 2, 3, 5, and 10 eV (lowest to highest curve).

OFMD results were benchmarked against QMD calculations at 5.0 and 12.5 g/cm^3.

The OFMD mutual-diffusion coefficients and viscosities all agree with the QMD results to within estimated uncertainties. The greatest differences (13% and 25% for mutual diffusion and viscosity, respectively) are seen at the highest temperature and density (10 eV, 12.5 g/cm^3). The OFMD electronic pressures agree with the QMD results to within 15% or better for $\rho=5$ g/cm^3 and 5% or better for $\rho=12.5$ g/cm^3. Thus, we conclude that the simpler OFMD method can be used with confidence in the warm dense matter regime considered.

The OCP results [36] for mutual diffusion agree with the QMD results at low temperatures (2 and 3 eV). However, as the temperature increases the OCP results underestimate the QMD results, e.g., by 30% at $T=10$ eV.

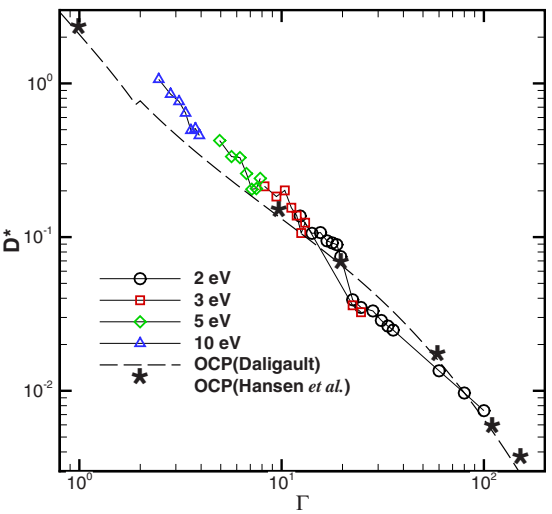

FIG. 9. (Color online) Reduced diffusion coefficient vs Γ for the D-T mixture calculated using OFMD at the indicated temperatures. The OCP model results of Daligault [36] (dashed curve, discontinuous at $\Gamma=2$) and Hansen *et al.* [40] (asterisks) are shown for comparison.

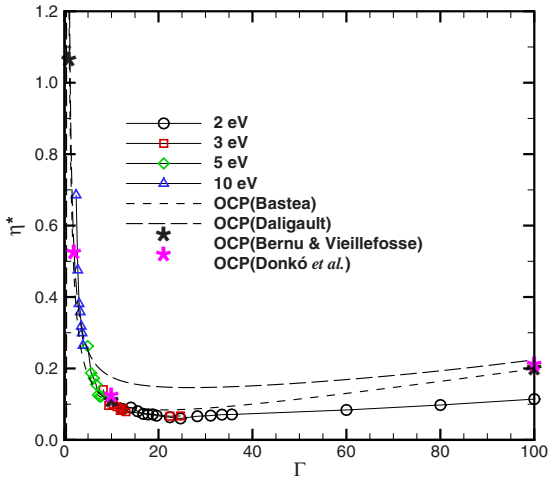

FIG. 10. (Color online) Reduced viscosity vs Γ for the *D-T* mixture calculated using OFMD at the indicated temperatures. The OCP model results of Bastea [37] (short-dashed curve), Daligault [36] (long-dashed curve), Bernu and Vieillefosse [43] (black asterisks), and Donkó *et al.* [44] (purple (gray) asterisks) are shown for comparison.

For viscosity the OCP model [36,37] is not as good as for diffusion, especially at the lower density 5.0 g/cm^3 where the model gives a temperature dependence significantly different from that of the QMD and OFMD results. Simple formulas for the viscosity based on kinetic theory by Wallenborn and Baus [38] show larger deviations though they display the qualitatively correct behavior.

The Yukawa screening modification of the OCP model proposed by Murillo [41] worsens the agreement of diffusion and viscosity with the QMD/OFMD results in all cases in the treated regime. The QMD excess pressures (due to electronic exchange and correlation) are 4–12 % smaller (in magnitude) than derived from the TCP model of Ichimaru *et al.* [45]. The deviation of the OFMD pressures from the TCP model are somewhat larger (15–21 %).

The OFMD mass-scaled self-diffusion coefficients for D compared with T are equal to within a few percent or better. The average of the D and T self-diffusion coefficients equals the mutual-diffusion coefficient to within 10% or better.

The OFMD reduced viscosities agree with all [37,42–44] OCP results (except one [36]) to within ~15% for Γ between 2.5 and 36. For $\Gamma > 36$, the OFMD results increase more slowly than the OCP results as a function of increasing Γ, the deviation reaching a factor of almost 2 at $\Gamma = 100$. The agreement with the Daligault [36] OCP calculation is not nearly as good.

The reduced diffusion and viscosity coefficients are found to depend largely, though not completely, only on the Coulomb coupling parameter Γ, with a minimum in the reduced viscosity at $\Gamma \approx 25$, approximately the same position found in the OCP simulations.

ACKNOWLEDGMENTS

This work was supported by the Advanced Simulation and Computing Program. The Los Alamos National Laboratory is operated by Los Alamos National Security, LLC for the National Nuclear Security Administration of the U.S. Department of Energy under Contract No. DE-AC52-06NA25396.

[1] H. F. Robey, Y. Zhou, A. C. Buckingham, P. Keiter, B. A. Remington, and R. P. Drake, Phys. Plasmas **10**, 614 (2003).
[2] P. Amendt, J. D. Colvin, J. D. Ramshaw, H. F. Robey, and O. L. Landen, Phys. Plasmas **10**, 820 (2003).
[3] J. L. Milovich, P. Amendt, M. Marinak, and H. Robey, Phys. Plasmas **11**, 1552 (2004).
[4] L. A. Collins, J. D. Kress, D. L. Lynch, and N. Troullier, J. Quant. Spectrosc. Radiat. Transf. **51**, 65 (1994).
[5] I. Kwon, J. D. Kress, and L. A. Collins, Phys. Rev. B **50**, 9118 (1994).
[6] L. Collins, I. Kwon, J. Kress, N. Troullier, and D. Lynch, Phys. Rev. E **52**, 6202 (1995).
[7] J. G. Clérouin and S. Bernard, Phys. Rev. E **56**, 3534 (1997).
[8] I. Kwon, L. Collins, J. Kress, and N. Troullier, EPL **29**, 537 (1995).
[9] J. Clérouin and J.-F. Dufrêche, Phys. Rev. E **64**, 066406 (2001).
[10] G. Zérah, J. Clérouin, and E. L. Pollock, Phys. Rev. Lett. **69**, 446 (1992).
[11] F. Lambert, J. Clérouin, and S. Mazevet, EPL **75**, 681 (2006).
[12] F. Lambert, J. Clérouin, and G. Zérah, Phys. Rev. E **73**, 016403 (2006).
[13] D. A. Horner, F. Lambert, J. D. Kress, and L. A. Collins, Phys. Rev. B **80**, 024305 (2009).
[14] G. Kresse and J. Hafner, Phys. Rev. B **47**, 558 (1993).
[15] G. Kresse and J. Furthmuller, Comput. Mater. Sci. **6**, 15 (1996).
[16] G. Kresse and J. Furthmuller, Phys. Rev. B **54**, 11169 (1996).
[17] P. H. Hünenberger, Adv. Polym. Sci. **173**, 105 (2005); D. J. Evans and B. L. Holian, J. Chem. Phys. **83**, 4069 (1985).
[18] R. M. Martin, *Electronic Structure: Basic Theory and Practical Methods* (Cambridge University Press, Cambridge, England, 2004).
[19] J. P. Perdew, J. A. Chevary, S. H. Vosko, K. A. Jackson, M. R. Pederson, D. J. Singh, and C. Fiolhais, Phys. Rev. B **46**, 6671 (1992).
[20] J. Clerouin, E. L. Pollock, and G. Zerah, Phys. Rev. A **46**, 5130 (1992).
[21] S. Mazevet, F. Lambert, F. Bottin, G. Zérah, and J. Clérouin, Phys. Rev. E **75**, 056404 (2007).
[22] F. Lambert, J. Clérouin, J.-F. Danel, L. Kazandjian, and G. Zérah, Phys. Rev. E **77**, 026402 (2008).
[23] S. Ichimaru, *Statistical Plasma Physics, Vol. II: Condensed Plasmas* (Addison-Wesley, Reading, MA, 1994), Appendix B.
[24] P. Hohenberg and W. Kohn, Phys. Rev. **136**, B864 (1964).
[25] M. Brack and R. K. Bhaduri, *Semiclassical Physics* (Westview Press, Boulder, Colorado, 2003).
[26] J. P. Perdew and A. Zunger, Phys. Rev. B **23**, 5048 (1981).

[27] G. Faussurier, P. L. Silvestrelli, and C. Blancard, High Energy Density Phys. **5**, 74 (2009).
[28] F. Perrot, Phys. Rev. A **20**, 586 (1979).
[29] P. Minary, G. J. Martyna, and M. E. Tuckerman, J. Chem. Phys. **118**, 2510 (2003); **118**, 2527 (2003).
[30] P. Vieillefosse and J. P. Hansen, Phys. Rev. A **12**, 1106 (1975).
[31] J. P. Hansen and I. R. McDonald, *The Theory of Simple Liquids*, 2nd ed. (Academic Press, New York, 1986), Chap. 8.
[32] M. Schoen and C. Hoheisel, Mol. Phys. **52**, 33 (1984); **52**, 1029 (1984).
[33] D. B. Boercker and E. L. Pollock, Phys. Rev. A **36**, 1779 (1987).
[34] M. P. Allen and D. J. Tildesley, *Computer Simulation of Liquids* (Oxford University Press, New York, 1989).
[35] R. Zwanzig and N. K. Ailawadi, Phys. Rev. **182**, 280 (1969).
[36] J. Daligault, Phys. Rev. Lett. **96**, 065003 (2006); **103**, 029901(E) (2009).
[37] S. Bastea, Phys. Rev. E **71**, 056405 (2005).
[38] J. Wallenborn and M. Baus, Phys. Rev. A **18**, 1737 (1978).
[39] J. P. Hansen, G. M. Torrie, and P. Vieillefosse, Phys. Rev. A **16**, 2153 (1977).
[40] J. P. Hansen, I. R. McDonald, and E. L. Pollock, Phys. Rev. A **11**, 1025 (1975).
[41] M. S. Murillo, Phys. Rev. E **62**, 4115 (2000).
[42] F. Lambert, Ph.D. thesis, Université Paris XI–Commissariat à l'Énergie Atomique, 2007.
[43] B. Bernu and P. Vieillefosse, Phys. Rev. A **18**, 2345 (1978).
[44] Z. Donkó, B. Nyíri, L. Szalai, and S. Holló, Phys. Rev. Lett. **81**, 1622 (1998); Z. Donkó and B. Nyíri, Phys. Plasmas **7**, 45 (2000).
[45] S. Ichimaru, H. Iyetomi, and S. Tanaka, Phys. Rep. **149**, 91 (1987).
[46] J. P. Hansen, F. Joly, and I. R. McDonald, Physica A **132**, 472 (1985).
[47] J. G. Clérouin, M. H. Cherfi, and G. Zérah, EPL **42**, 37 (1998).